

Morphology and toughening mechanisms in clay-modified styrene-butadiene-styrene rubber-toughened polypropylene

YANMEI LI, GUANG-XUE WEI, HUNG-JUE SUE*

*Polymer Technology Center, Department of Mechanical Engineering,
Texas A&M University, College Station, TX 77843-3123, USA
E-mail: hjsu@acs.tamu.edu*

Clay-modified styrene-butadiene-styrene (SBS) rubber is utilized to toughen polypropylene (PP). The SBS rubber is found to have good compatibility with clay particles. SBS rubber helps to finely disperse clay particles in PP matrix. Mode-I fracture mechanisms are investigated using optical microscopy and transmission electron microscopy techniques. Rubber particle cavitation and matrix shear yielding are found to be the main toughening mechanisms in PP/SBS system. In the case of PP/SBS/clay system, widespread rubber particle cavitation, which appears to be facilitated by the presence of clay particle inclusions inside the SBS rubber particles, takes place in the PP matrix. This, in turn, leads to the formation of a bigger shear yielded zone in PP matrix. As a result, an enhanced toughness is observed. © 2002 Kluwer Academic Publishers

1. Introduction

Polypropylene (PP) is widely used in packaging, textile, household goods, and automobile applications because of its good processability, relatively high performance, great recyclability and low cost characteristics. However, the ability for PP to be utilized as an engineering thermoplastic is still limited by its low modulus and poor impact resistance. To expand engineering usage of PP, extensive efforts on toughening of PP have been carried out in the past twenty years [1–24].

Rubber modification is a well-known approach for toughening PP [1–10]. It has been shown that rubber particle cavitation, crazing and shear yielding are among the major toughening mechanisms found in rubber-modified PP [1–6]. Rubber particles can act as stress concentrators to initiate and terminate crazes [2–5] or can undergo internal cavitation to relieve the triaxial stress state in front of the crack tip [6–8, 11–13]. Widespread rubber particle cavitation and massive crazing can facilitate shear yielding of the PP matrix [4, 5]. The toughening mechanism(s) that may operate in PP depends on the rubber type, size, content, and the level of interfacial adhesion between rubber particles and the PP matrix [1–10]. For example, for the ethylene-propylene-diene monomer (EPDM) toughened PP system, Jang *et al.* [1] suggest that EPDM particles could effectively nucleate crazes in PP if the particle size is above 0.5 μm . However, van der Wal *et al.* [8] indicate that EPDM particle cavitation is the key mechanism leading to a toughened PP. They claim that large rubber particles (1.6 μm) are more effective

in relieving the plane strain constraint since they contain several internal cavities, instead of only one cavity found in small rubber particles. No crazing was found in the PP/EPDM blends they studied.

Rigid-rigid polymer toughening approach has been shown to be an alternative means for toughening PP [14–17]. The roles of the toughener phase are to generate numerous stress concentration sites and to relieve triaxial stress in front of the crack tip, thus promoting shear plastic deformation in the PP matrix. In contrast to the rubber toughening approach, this approach does not cause reduction in modulus. The main drawbacks of this approach are its ineffectiveness, as opposed to rubber toughening, in improving low temperature impact strength and ductile-brittle transition temperature. Consequently, rubber toughening is still preferred for applications where good low temperature impact strength and low ductile-brittle transition temperature are critical. Although toughness can be greatly improved in PP blends through rubber toughening, the accompanying penalty from this approach usually results in a noticeable reduction in stiffness [1–8]. Organic fillers are known to be effective in improving strength and modulus of polymers [18–20]. However, a decrease in toughness usually ensues. Interestingly, the incorporation of both inorganic fillers and rubber particles has been shown to improve both stiffness and toughness of PP [21–24]. It has been shown that two typical types of morphological characteristics are generally present in a three-component PP/rubber/filler blend [21–24]. They are: (1) the toughener phase and filler phase are

*Author to whom all correspondence should be addressed.

independently dispersed in PP and (2) the filler phase resides inside the toughener phase. It is generally agreed that the elastic modulus can be increased if the filler phase and the toughener phase are separated from each other in the blend [23]. Also, the impact properties of the blend will increase if the filler phase resides inside the toughener phase, forming a core-shell morphology in the blend [21, 22, 24].

So far, few systematic studies have been carried out on the fundamental understanding of the toughening process in three-component PP/rubber/filler blends. There are still questions as to how the filler, the rubber and the filler-containing rubber phases affect PP toughening. The main objective of this study is to investigate the operating toughening mechanism (s) in such a multi-phase PP blend system.

Clay-modified styrene-butadiene-styrene (SBS) rubber is chosen as the model PP system for the present study. The fracture mechanism analysis is performed on the double-notch four-point-bend (DN-4PB) specimens using transmitted optical microscopy (TOM) and transmission electron microscopy (TEM) to gain insight into the toughening mechanisms that are responsible for the toughening of PP. The toughening mechanisms observed in the multi-phase PP/SBS/clay blend are compared with other toughened PP blends found in the literature.

2. Experimental

2.1. Materials

The PP chosen in this research is isotactic PP that has $M_n = 100,000$ and $M_w = 368,000$ with a melt flow index (MFI) of 2.5. Kaolinite clay, which had been surface treated with dimethyl sulfoxide, was chosen as the filler phase. SBS was selected as the rubber phase. SBS (YH-792) is a linear elastomer obtained from Beijing YanHua Petrochemical C. Ltd., China, which has 40 wt% styrene. The M_n of SBS is about 100,000. The PP/SBS/clay (92/5/3 ratio by weight) blend was prepared via pre-mixing of rubber and clay, followed by mixing with PP using a research grade two-roll milling machine at a roll temperature of 200°C. For comparison purposes, neat PP, PP/clay (97/3 ratio by weight) and PP/SBS (95/5 ratio by weight) blends were also prepared under the same processing condition. The testing plaques were compression-molded at 200°C and prepared for morphology characterization and mechanical property testing.

2.2. Specimen preparation

Single-edge-notch three-point-bend (SEN-3PB) specimens were cut from the compression molded plaques. Samples were machined to reach the final dimensions of $63.5 \times 12.7 \times 4 \text{ mm}^3$. The SEN-3PB specimens were notched with a 250 μm radius notch cutter to a notch depth of 5.5 mm, followed by liquid nitrogen-chilled razor blade tapping to wedge open a sharp crack to a total depth of about 6.4 mm ($a/W = 0.5\text{--}0.55$) for J -integral fracture toughness measurements.

The double-notch four-point-bend (DN-4PB) specimens were prepared to generate a sub-critically propa-

gated crack for detailed damage mechanism investigations. In the DN-4PB specimens, two nearly identical cracks were prepared with care. Specimens were tested at the speed of 50.8 mm/min using Instron (Model 4411) at room temperature. During the test, care was taken to ensure that the two inner loading points contact the specimen simultaneously while the specimen was supported at the outer loading points.

2.3. Dynamic mechanical behavior

The dynamic mechanical analysis (DMA) of the neat and PP blends were conducted using Rheometrics RMS-800 in a torsional mode, with 2.5°C per step. A constant strain amplitude of 0.1% and a fixed frequency of 1 Hz were employed. The samples were tested at temperatures ranging from -140°C to 170°C . The temperature at which the maximum $\tan \delta$ value is located is assigned as the glass transition temperature (T_g).

2.4. DSC measurements

Differential scanning calorimetry (DSC) measurements were performed in nitrogen atmosphere at a heating/cooling rate of $10^\circ\text{C}/\text{min}$. The melting temperature was determined from the heating curve. The heat of fusion of 100% PP crystal was taken as 209 J/g for crystallinity calculation [25]. The crystallinity of PP in PP blends was calculated using the following equation:

$$X'_c = \frac{X_c}{\text{weight percentage of PP in the blends}}$$

where X_c is the crystallinity of PP blends and X'_c is the crystallinity of neat PP.

2.5. Wide angle X-ray scattering (WAXS)

A Sintag Pad V X-ray Diffractometer was used to study WAXS pattern of PP blends. Testing was carried out with 2θ scanned between 2° and 30° at $1^\circ/\text{min}$ scanning rate and 0.04 chopper increment, using Cu K_α ($\lambda = 0.15418 \text{ nm}$) radiation. Specimens with dimensions of $30 \times 12 \times 3$ (length \times width \times thickness) mm^3 were used.

2.6. J -integral test

The J -integral test was conducted according to the ASTM standard D-6068 using a multiple-specimen technique at room temperature. A screw-driven mechanical testing machine (Instron, Model 4411) was used to perform the test at a crosshead speed of 2 mm/min. During the test, a series of SEN-3PB specimens were loaded and unloaded to different predetermined deflections, i.e., different levels of crack growth. The load-deflection curve was recorded and integrated to calculate the energy required to extend the crack, which corresponds to the area under the load-deflection diagram. After testing, each specimen was immersed in liquid nitrogen for 3 minutes and broken immediately to

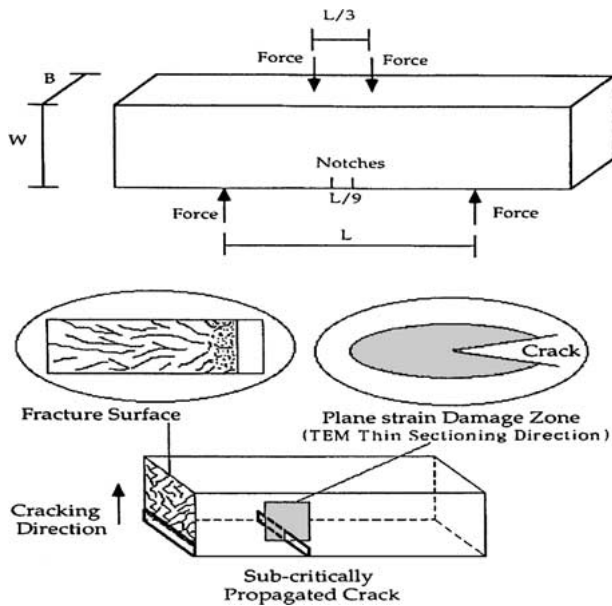


Figure 1 Schematic of a DN-4PB specimen and the regions utilized for microscopy analysis.

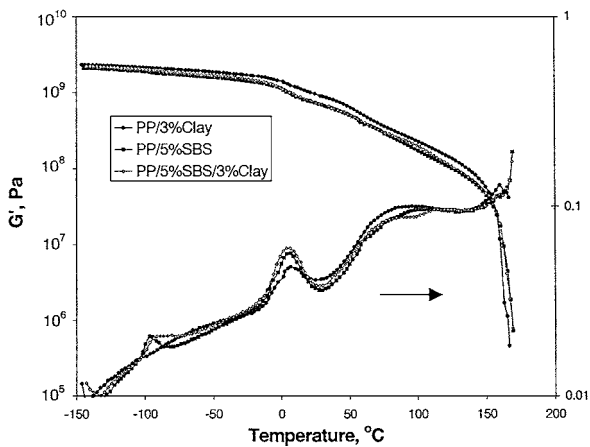


Figure 2 Dynamic mechanical analysis of PP blends.

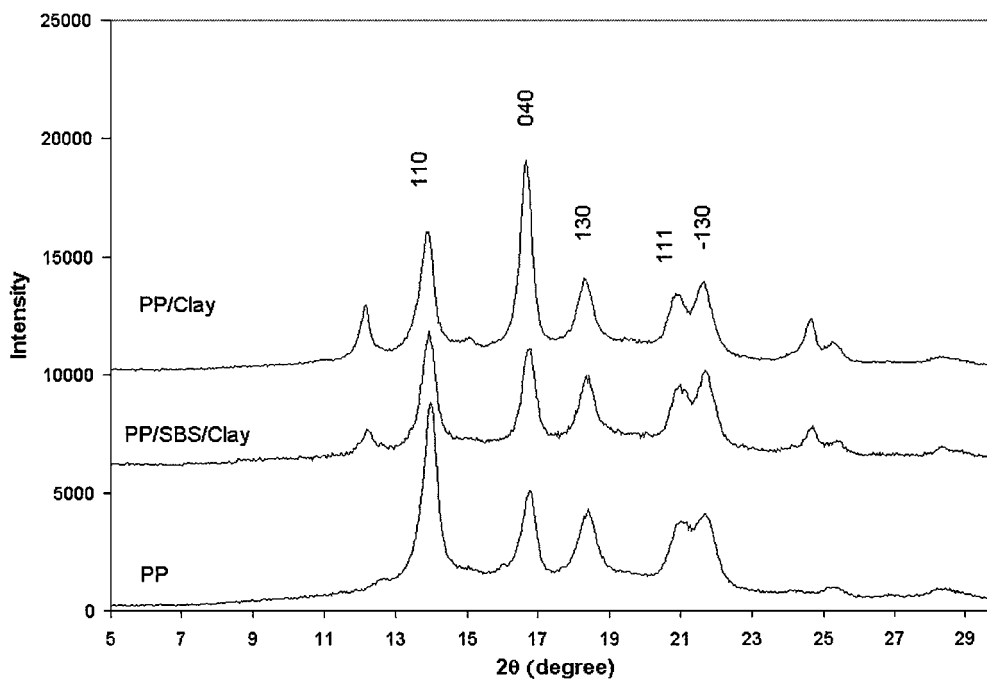


Figure 3 WAXS spectra of PP and PP blends.

cause brittle fracture. The extent of crack growth was measured from the fracture surface using an optical microscope. The J -integral value was calculated using the following equation:

$$J = \frac{2U}{B(W - a)}$$

where U is the energy required for crack propagation, B is the thickness of the specimen, W is the width of the specimen, and a is the initial crack length.

The calculated J -values were then plotted against the advanced crack length, Δa , to obtain a J - R curve. The J_C value was determined at the point of intersection between the J - R curve and the blunting line ($J = 2\sigma_y \Delta a$, where σ_y is the yield stress).

2.7. Flexural modulus measurement

The three-point-bend flexural moduli of PP blends were measured according to the ASTM standard D-790 (Method I). An Instron (Model 1125) screw-driven mechanical testing machine was used to perform the measurement at a crosshead speed of 5 mm/min and a span-to-depth ratio of 16. The bending modulus of elasticity was calculated using the equation: $E = L^3 m / (4bd^3)$, where L is the support span, b is the width of beam, d is the depth of beam, and m is the slope of the tangent to the initial straight-line portion of the load-deflection curve. At least three specimens were used for each system.

2.8. Microscopy

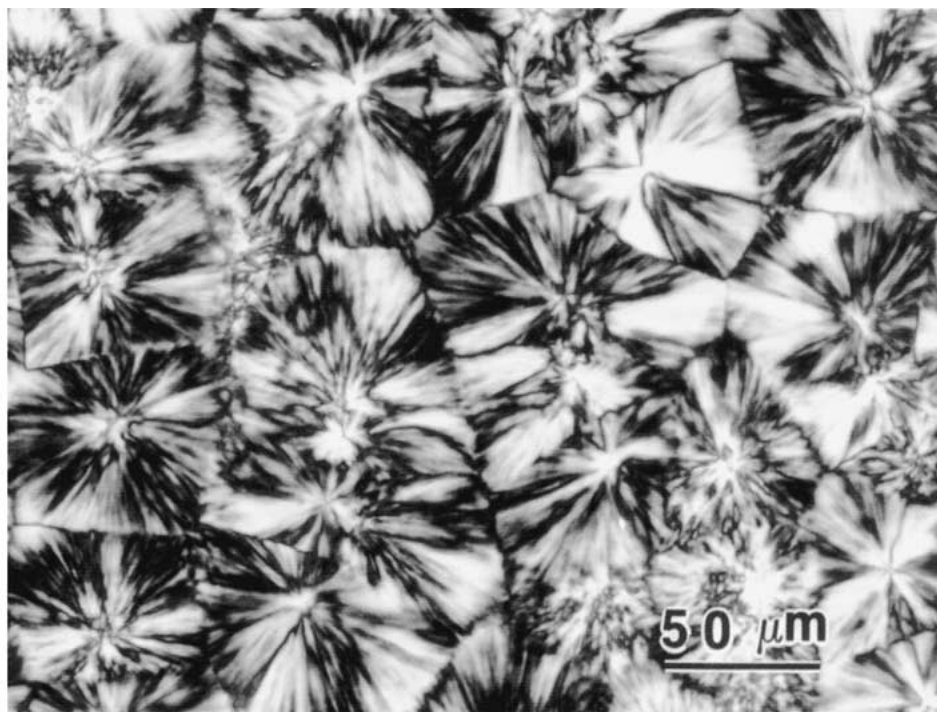
The morphology of PP and its blends was characterized using TOM and TEM. In the TOM investigation, samples were polished to about 20 μm in thickness. Spherulites in neat PP and PP blends were characterized

using an Olympus-BX60 optical microscope under cross-polarization light.

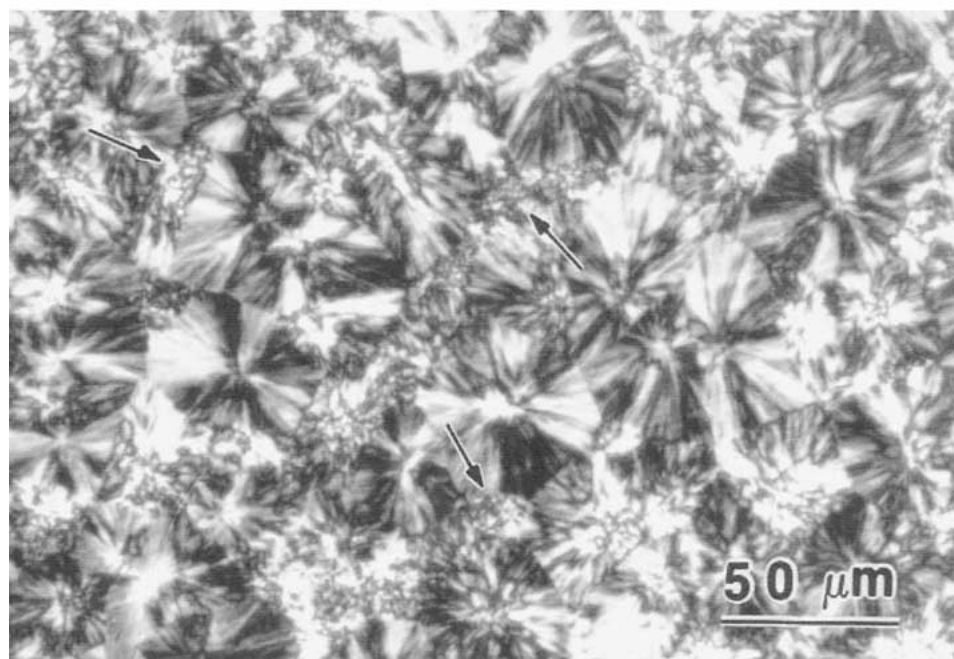
For the TEM sample preparation, specimens were carefully trimmed to an appropriate size ($5 \times 5 \text{ mm}^2$) and embedded in a diglycidyl ether of bisphenol-A (DGEBA) epoxy and diethylenetriamine system (12 : 1 ratio by weight). The epoxy was then cured at room temperature overnight. The cured block was further trimmed to a size of about $0.3 \times 0.3 \text{ mm}^2$. A diamond knife was used to face off the trimmed block prior to RuO_4 straining. The faced-off block was exposed to the vapor of an aqueous RuO_4 solution (0.5% by weight) for

2.5 hrs. Ultra-thin sections, ranging from 60 to 80 nm, were obtained using a Reichert-Jung Ultracut E microtome with a diamond knife at room temperature. The thin sections were placed on 200-mesh formvar-coated copper grids and examined using a JEOL 2000 FX ATEM operated at an accelerating voltage of 100 kV.

The DN-4PB damage zone of the subcritically propagated crack was cut along the crack propagation direction but perpendicular to the fracture surface using a diamond saw (Fig. 1). The plane strain core region of the crack tip damage zone was prepared for TOM and TEM investigations.

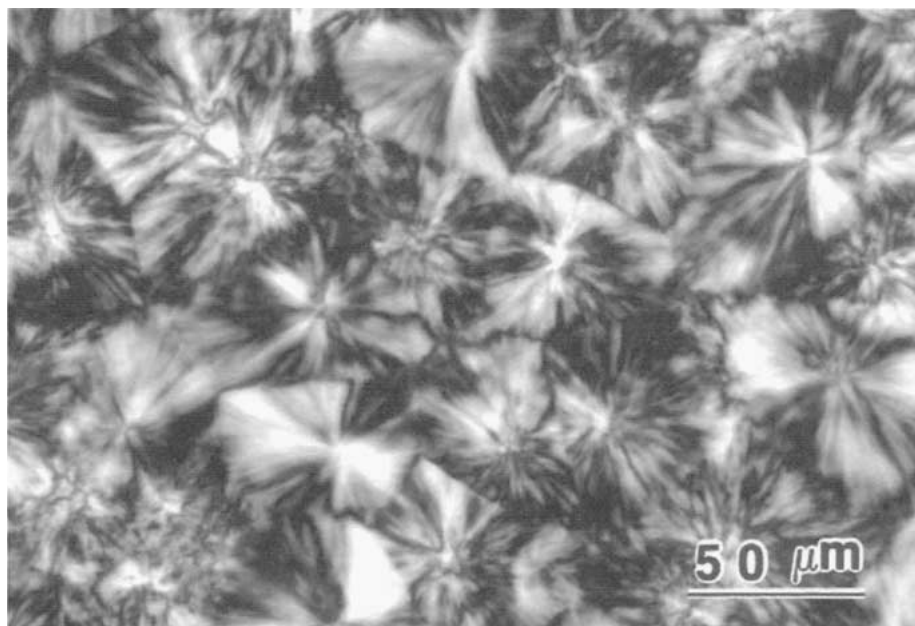


(a)

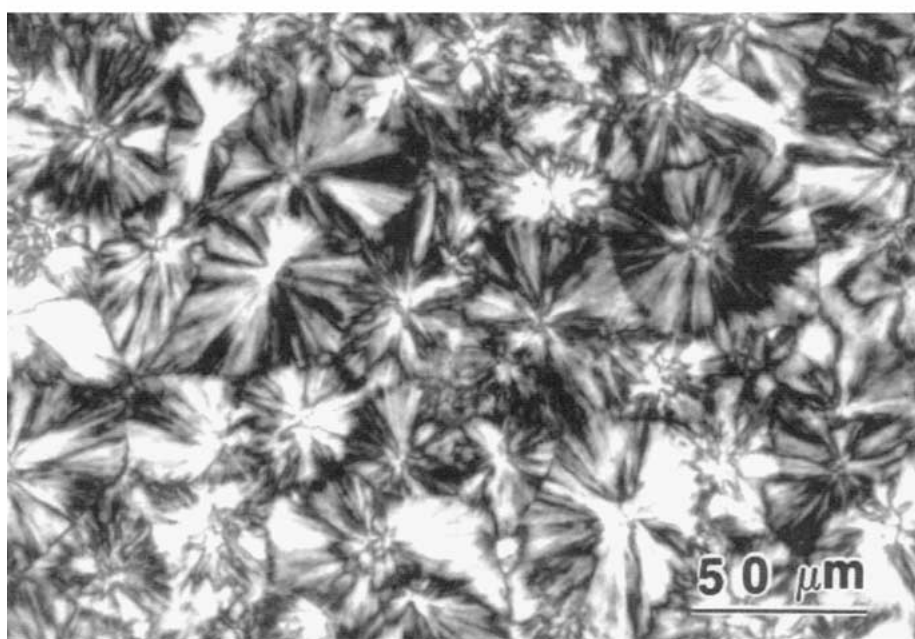


(b)

Figure 4 TOM taken under cross-polarized light. (a) PP; (b) PP/clay; (c) PP/SBS; (d) PP/SBS/clay. (Continued).



(c)



(d)

Figure 4 (Continued).

3. Results and discussion

3.1. Thermal analysis

The crystallinity of semi-crystalline polymers is believed to have a significant effect on mechanical property and fracture behavior in polymers. It is found that the crystallinity of PP is increased with the addition

of rubber and clay particles (Table I). Especially in the case of PP/clay, the crystallinity of PP is increased from about 40% to 47%. This suggests that clay particles can act as an effective nucleation agent. The melting temperatures of neat PP and the PP blends are all about the same.

TABLE I Selected properties of neat PP and PP blends

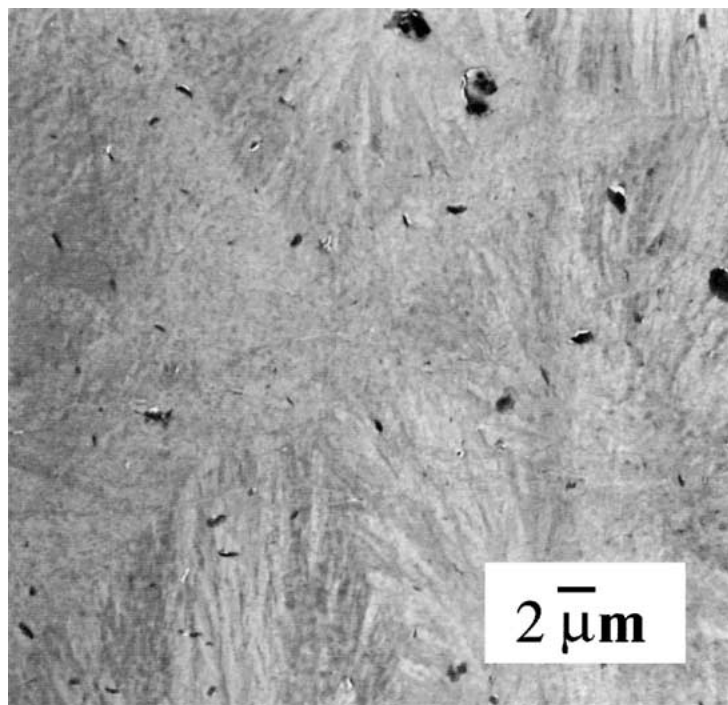
Materials	X_c (%)	T_g (°C)		G' (MPa)		Flexural modulus (GPa)	J_C (kJ/m ²)
		PP	SBS	25°C	80°C		
Neat PP	39.7	5.6	–	780	270	1.76 ± 0.02	3.0
PP/3%Clay	47.2	6.9	–	960	320	2.12 ± 0.05	1.9
PP/5%SBS	43.5	6.9	–97	730	260	1.47 ± 0.01	9.0
PP/5%SBS/3%Clay	44.3	6.4	–89	720	290	1.48 ± 0.03	10.5

3.2. Dynamic mechanical analysis

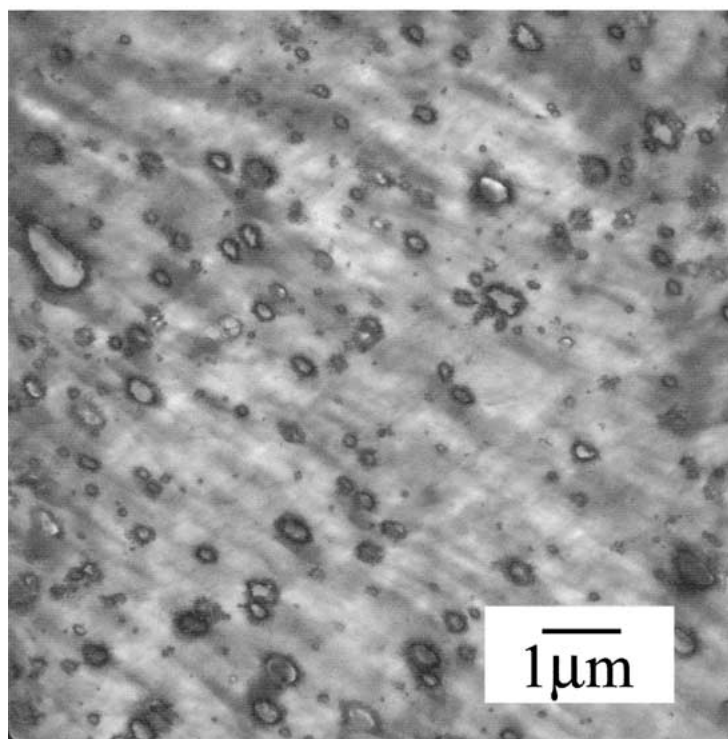
The dynamic mechanical spectra of PP, PP/clay, PP/SBS, and PP/SBS/clay are shown in Fig. 2. The T_g and selected shear storage moduli of all the blends are given in Table I. It is found that T_g of PP is about the same for all the blends studied. However, in the case of the PP/SBS/clay blend, the T_g of SBS is increased by about 8°C . Also, the curve of the $\tan \delta$ peak of SBS dampens after the incorporation of clay particles. This indicates that the SBS rubber is likely to have

molecularly interacted with the clay particles. In other words, some of the clay particles may have intercalated or exfoliated within the SBS phase. The good molecular interaction between SBS and clay can help improve dispersion and the interfacial adhesion between clay and PP matrix.

It should be noted that the shear storage moduli of PP are increased when 3% clay is added, especially at temperatures above the T_g of PP (i.e., 5.6°C). However, the shear storage moduli of PP are decreased when SBS

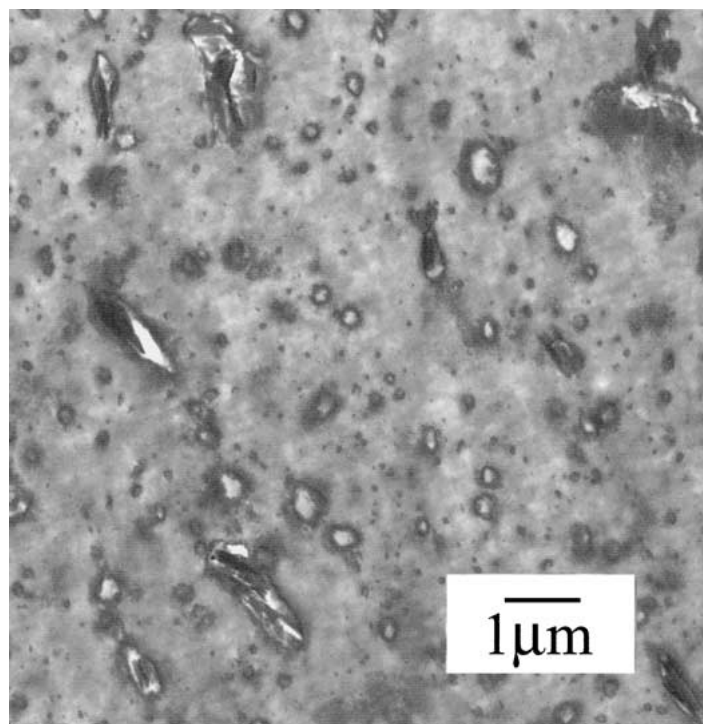


(a)



(b)

Figure 5 TEM morphology of PP blends. (a) PP/clay; (b) PP/SBS; (c) PP/SBS/clay. (Continued).



(c)

Figure 5 (Continued).

and SBS/clay are incorporated. However, it is noted that the moduli of PP/SBS/clay are increased at temperatures above 50°C.

3.3. WAXS analysis

WAXS spectra (Fig. 3) of PP and PP blends exhibit typical monoclinic α form crystalline structure [26]. The corresponding crystalline planes are marked on the plot. A reverse trend in relative intensities of (110) and (040) peaks is observed in PP/clay against those found in neat PP and PP/SBS/clay. It is unclear at this stage concerning the underlying cause(s) of such shifts in intensities between (110) and (040) peaks.

The diffraction peak ($2\theta = 12.24^\circ$) of clay observed in PP blends is the same as that found in the original clay. This indicates that the majority of clay particles still maintain its original crystalline structure form. However, careful investigation suggests that the clay peak intensity in PP/SBS/clay is much lower than that found in PP/clay. This suggests that part of the clay in PP/SBS/clay system has molecularly interacted with SBS rubber, and caused the original clay to either intercalate or exfoliate. The above findings agree well with the DMA results.

3.4. Morphology observation

Spherulite morphology in PP blends is characterized using TOM. TOM micrographs of polished thin-sections of PP and PP blends are shown in Fig. 4. The addition of the second phase particles results in a less regular spherulite texture with less well-defined spherulitic boundaries. The spherulite size in these PP blends is about 50 μm . Careful observation reveals that small

crystal clusters, which appear to be nucleated by clay particles, are present in the inter-spherulitic region (see arrows in Fig. 4b).

TEM is employed to further reveal the morphological details in PP blends (Fig. 5). In PP/clay blend, clay particles are found well-dispersed in the PP matrix (Fig. 5a). However, the particle size distribution ranges from nanometer size up to about 2 μm in size. Most of the clay particles appear to exhibit plate-like structure. In PP/SBS blend, the average rubber particle size is about 0.3 μm .

The PP/SBS/clay blend appears to contain two types of rubber particles: pure SBS particles and clay-containing SBS particles. In this blend, a unique core-shell particle morphology is observed. This is anticipated because SBS and clay were pre-mixed before blending with PP during sample preparation. All clay particles appear to be coated by SBS rubber. The size of clay particles appears to be greatly reduced even though a few 1 μm size clay particles are still occasionally observed.

It is noted that co-crystallization between SBS rubber and PP at the interface is observed in PP/SBS and PP/SBS/clay blends (Fig. 6). The co-crystallization at the interface may have helped promote sufficiently strong interfacial adhesion between SBS and PP as noted by Lu *et al.* [27]. Microscopy observations suggest that both SBS and clay particles are all well-dispersed in the PP blends investigated.

3.5. Mechanical properties

The flexural modulus of PP/clay is about 20% higher than that of neat PP, while the flexural moduli of both PP/SBS and PP/SBS/clay are about 20% lower than

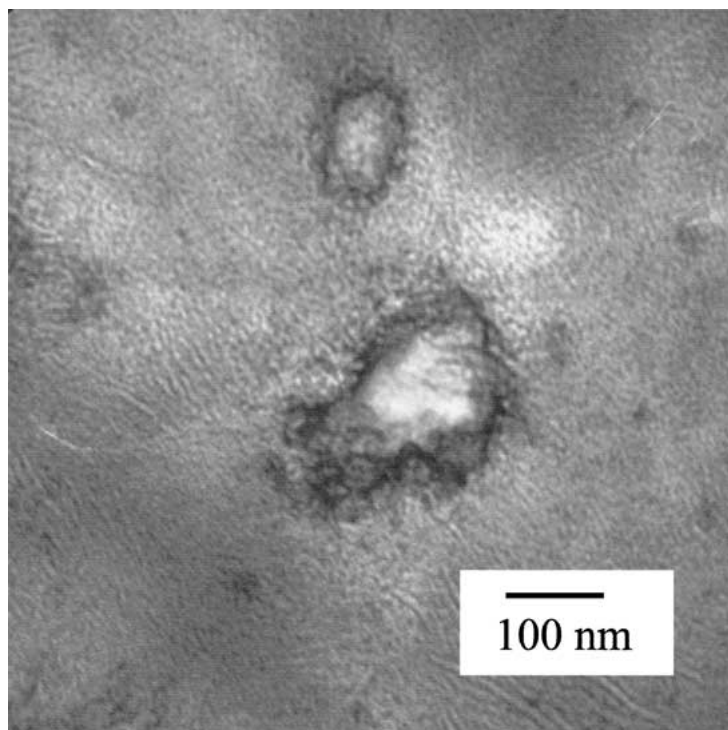


Figure 6 Co-crystallization at the interface between PP and SBS in PP/SBS blend.

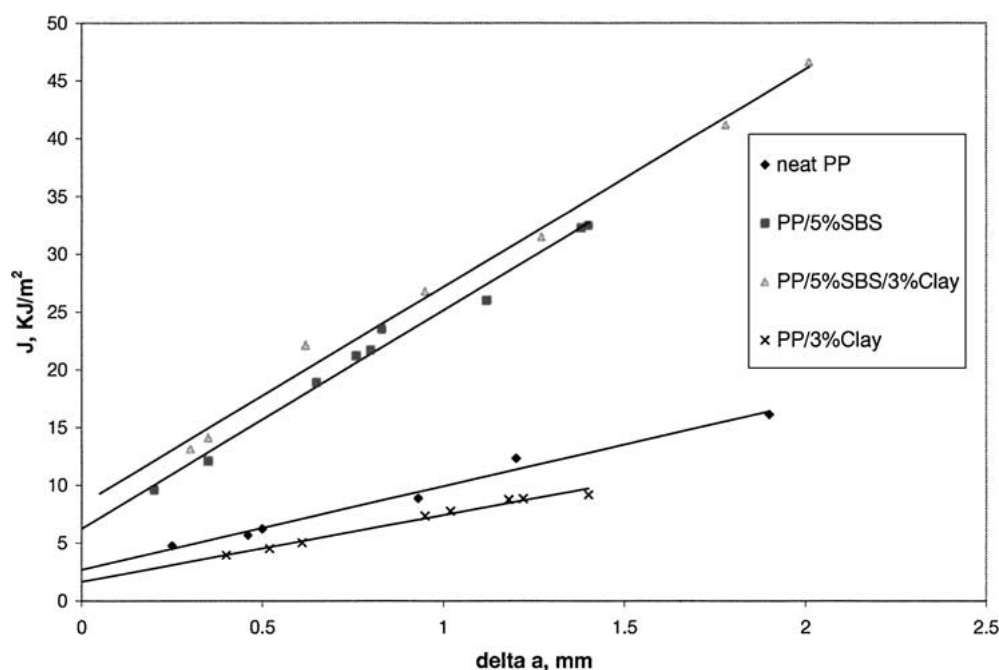


Figure 7 J - R curves of neat PP and PP blends.

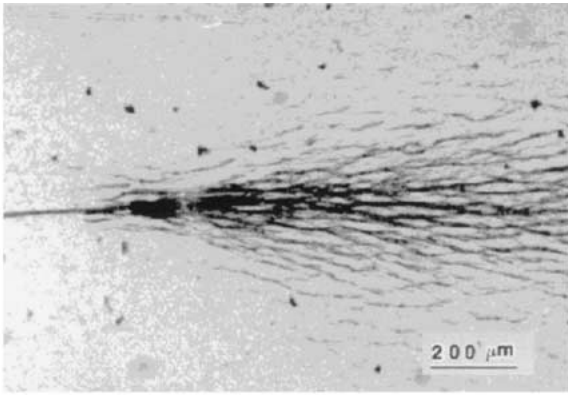
that of neat PP. This trend is consistent with the storage moduli results obtained from DMA experiments. It can be seen that the SBS-encapsulated clay particles are not effective in improving or maintaining the rigidity of PP matrix, but act more like rubber particles as a whole.

The toughness measurement results obtained from the J -integral experiments are shown in Table I and Fig. 7. It is clearly shown that the addition of clay alone lowers the toughness of PP significantly. The incorporation of 5% SBS into PP can greatly improve the toughness of PP. Interestingly, the PP/SBS/clay blend gives a slightly higher J_C value and a better crack prop-

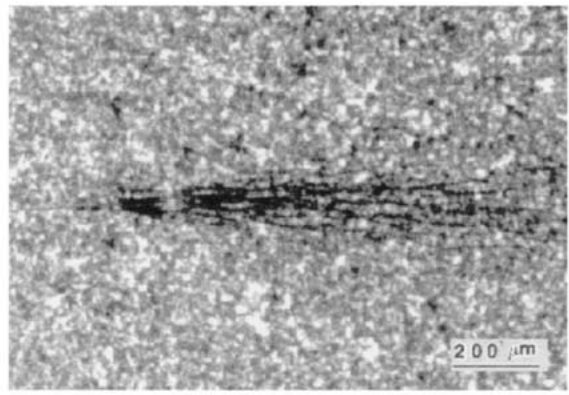
agation resistance (slope of J - R curve) than PP/SBS blend. In this study, only J_C values, instead of J_{IC} values, are reported because the specimen thickness of PP blends was insufficient to satisfy the ASTM standard requirements.

3.6. Toughening mechanisms investigation

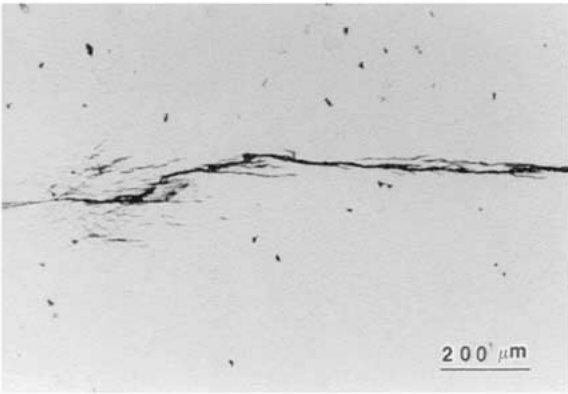
To better understand the operating toughening mechanisms in PP blends, TOM and TEM are utilized to examine the sub-fracture surface and the crack tip damage zone of the DN-4PB specimens. TOM provides an



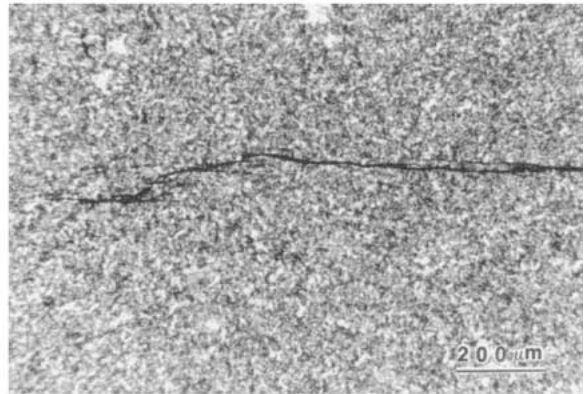
(a)



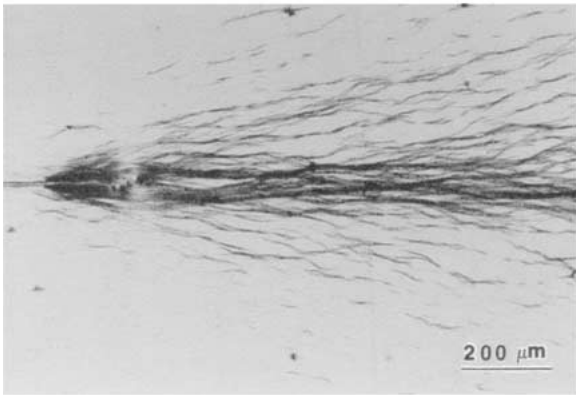
(b)



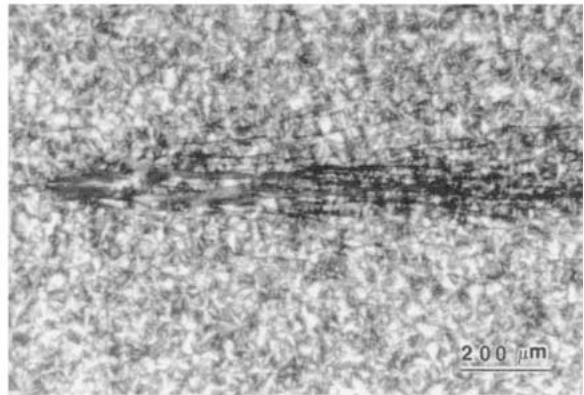
(c)



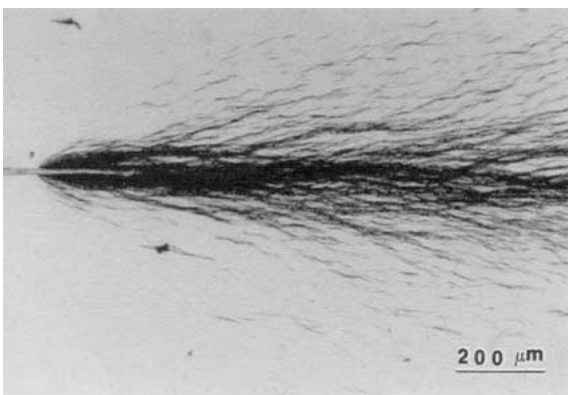
(d)



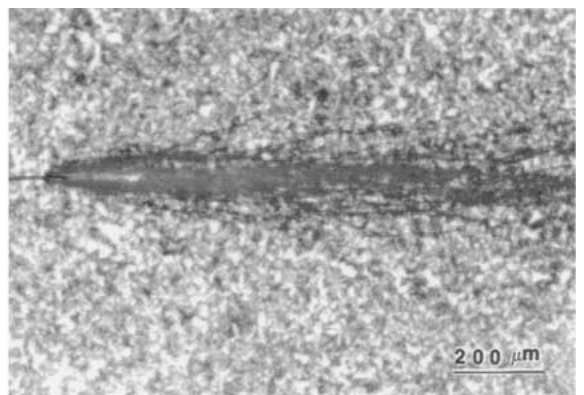
(e)



(f)



(g)



(h)

Figure 8 TOM of DN-4PB specimens (a) and (b) neat PP; (c) and (d) PP/clay; (e) and (f) PP/SBS; (g) and (h) PP/SBS/clay. (a), (c), (e) and (g) are under bright field; and (b), (d), (f) and (h) are taken under cross-polarized light (crack propagates from left to right).

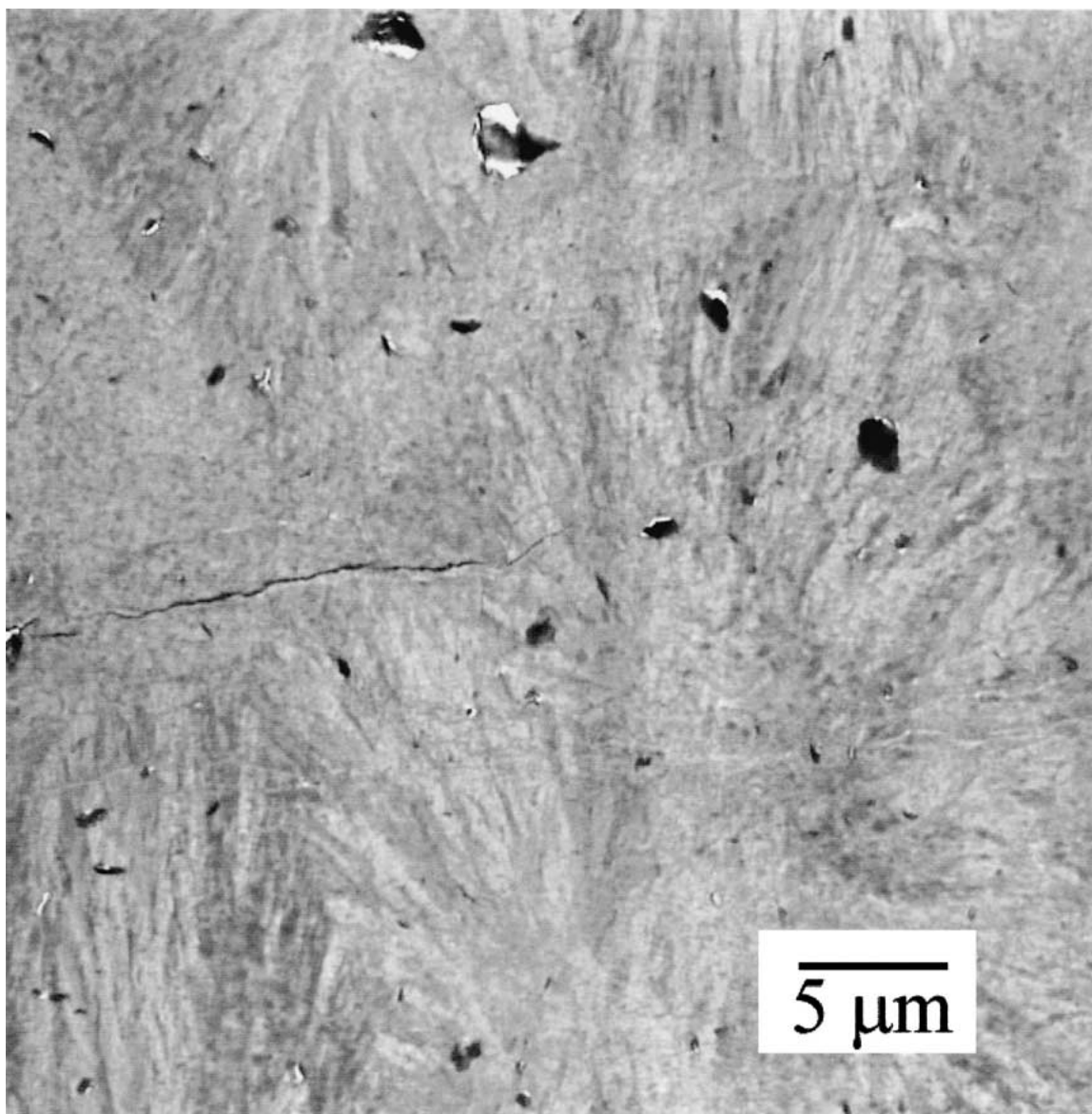
overview of the damage zone size in different PP blends (Fig. 8). The PP/clay blend shows a much smaller damage zone size than that of the neat PP system (Fig. 8c vs. 8a). No evidence of a birefringent zone was found. Only signs of crack deflection and crack bifurcation are observed. This finding agrees well with the low J_C value obtained for this blend. On the other hand, intense and large damage zones are formed in PP/SBS and PP/SBS/clay blends (Fig. 8e and g). Under cross-polarized light, large birefringent zones are observed in these two blends (Fig. 8f and h), which imply that shear yielding has taken place in these blends. The PP/SBS/clay blend contains the largest birefringent zone. This, again, is consistent with the J -integral measurements, which indicates that the PP/SBS/clay blend possesses higher crack initiation resistance and better crack propagation resistance than the PP/SBS system.

TEM is conducted on DN-4PB specimens to further probe the toughening mechanisms in different PP blends. TEM micrographs shown in Fig. 9 are taken at the crack tip regions of all the PP blends. In PP/clay

blend (Fig. 9a), as expected, no sign of crazing is found in this blend. Only crack deflection and crack bifurcation are observed. This explains why this blend is brittle. With the addition of SBS and SBS/clay particles, shear plastic deformation as illustrated by the highly deformed and elongated SBS particles around the crack tip is observed. Outside the plastic zone, rubber particle cavitation is found in PP/SBS and in PP/SBS/clay blends. Careful investigation suggests that the PP/SBS/clay blend has a larger and more intense shear plastic deformation zone than PP/SBS, which corresponds to the larger birefringence zone observed under TOM (Fig. 8h). No crazing is found in these two blends.

Fig. 10 is taken at about 30 μm beneath the fracture surface in PP/SBS/clay blend. The lower portion of the micrograph indicates the cavitation zone. The upper part of the micrograph shows the plastic zone as indicated by the highly stretched and elongated particles.

It is interesting to note that the shape of clay particles inside the plastic zone is much thinner (Fig. 9c)



(a)

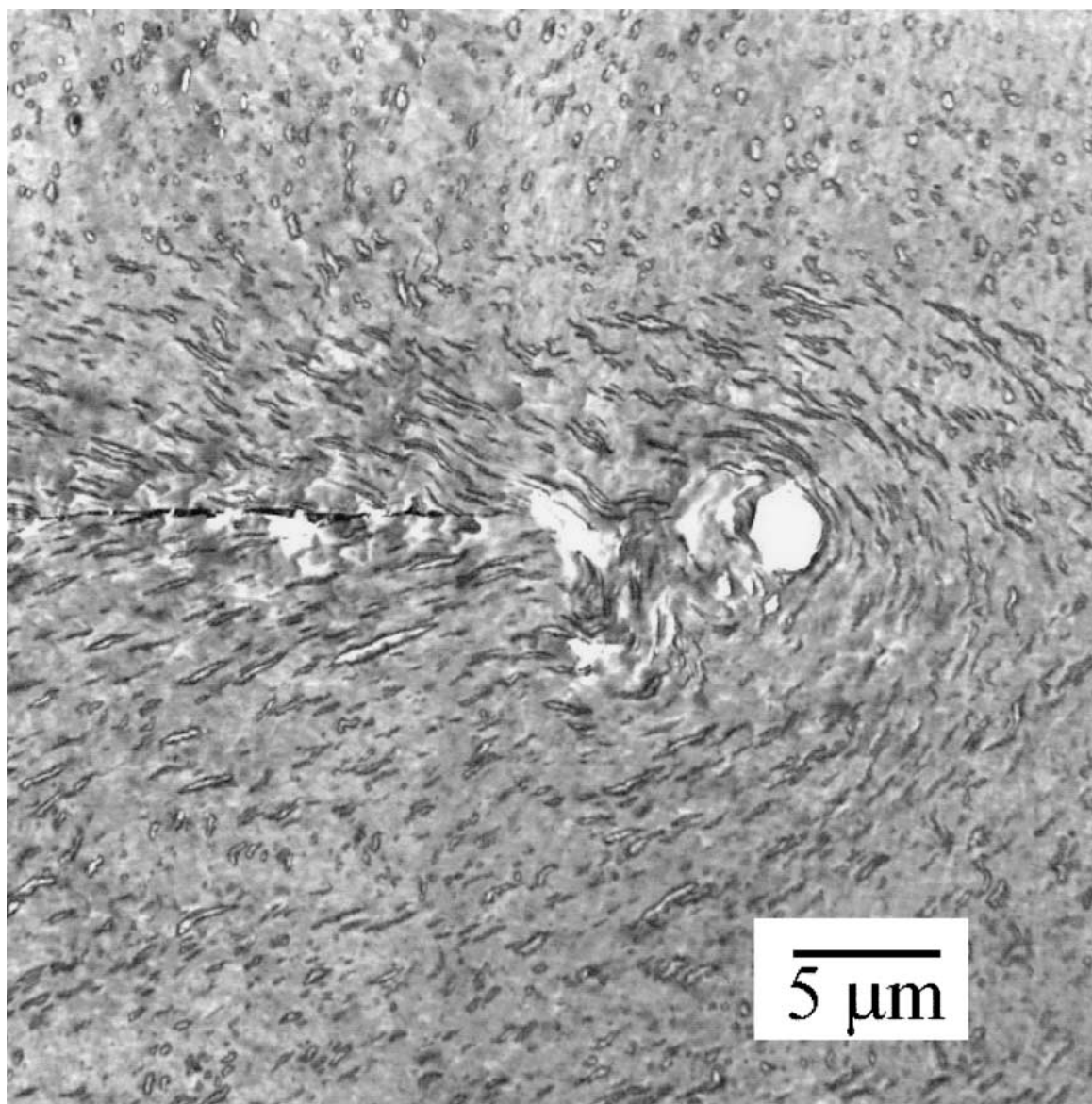
Figure 9 TEM of crack tip of DN-4PB specimens of PP blends. (a) PP/clay; (b) PP/SBS; (c) PP/SBS/clay. (Continued).

than those found in the undeformed region. We surmise that the shear deformation process at the crack tip can shear separate clay layers. This leads to the formation of finer clay particles with much thinner platelets inside the rubber phase. Crazeing has been recognized as the main fracture mechanism in neat PP [5, 14, 15]. However, no crazeing is found in all the PP blends investigated in this study. This suggests that either the crazeing stress of PP is higher than the stresses for SBS rubber cavitation and interfacial debonding or the SBS and SBS/clay particle sizes are simply too small to be effective in initiating crazeing in PP. The above finding is consistent with our earlier investigation on PP/noryl and PP/styrene-ethylene-propylene systems, which indicates that the most effective rubber particle size to initiate crazeing is between 0.7–1 μm [5, 14].

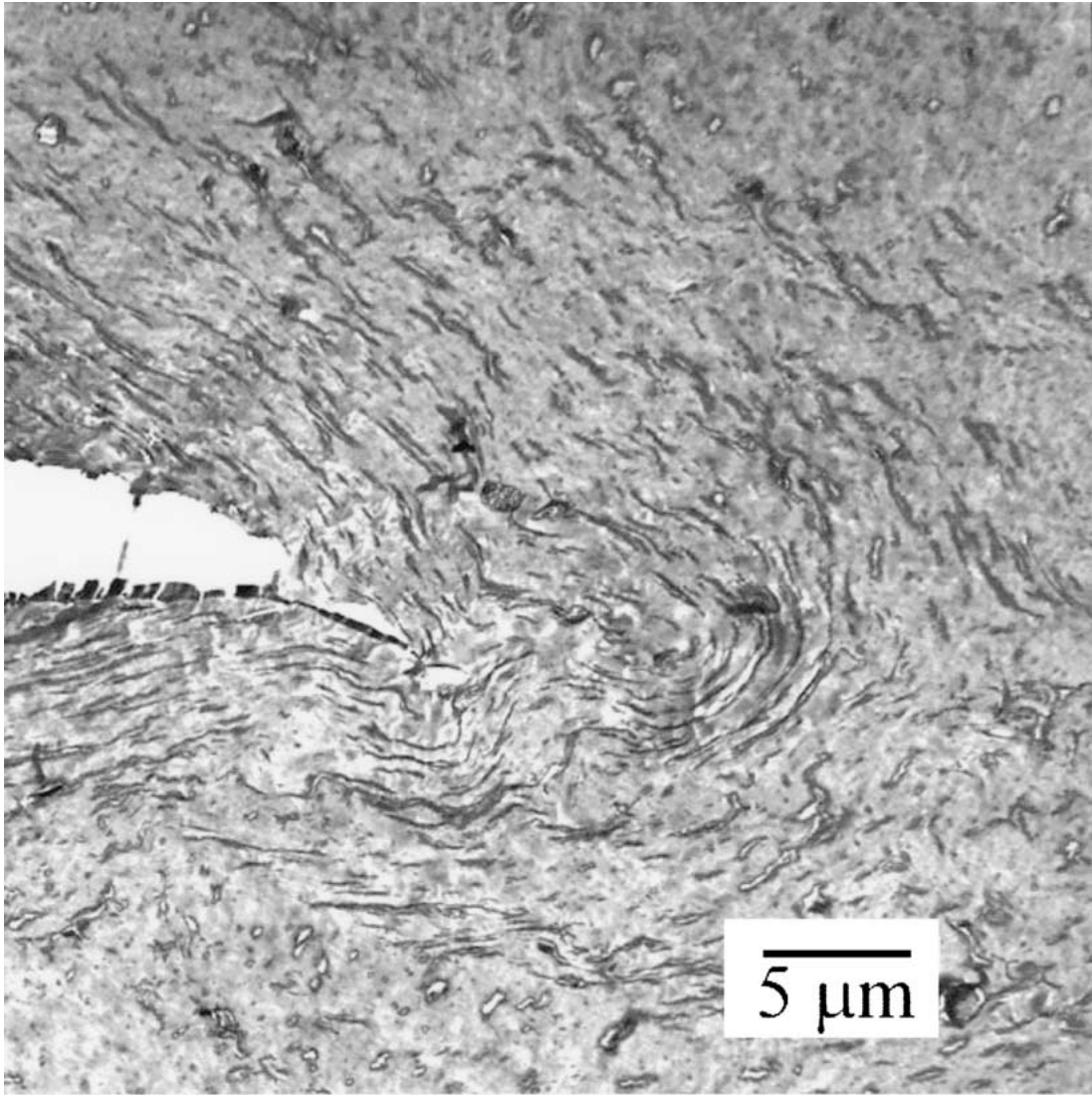
Toughener particle size, particle content, and the type of particles utilized are critical in triggering effective toughening mechanisms. Rubber particle cavitation is found in both PP/SBS and PP/SBS/clay blends (Fig. 9b

and c). In this study, it is evident that rubber cavitation occurs before shear yielding (Fig. 10). In contrast, only crazeing is found in PP/EPDM [1, 2, 6], PP/EPR [1, 4] and PP/SEP blends [5]. The discrepancy between the present findings and the PP/EPDM, PP/EPR, and PP/SEP systems investigated by others may be because of differences in rubber characteristics and rubber particle sizes.

The debonding (Fig. 10) between the clay inclusion and the encapsulating rubber phase in PP/SBS/clay, which is equivalent to the cavitation of SBS rubber, may have contributed to a more effective relief of the triaxial stress state around the crack tip. This allows PP to undergo a larger scale of plastic deformation. As shown in Fig. 8, a larger birefringence zone is observed in PP/SBS/clay blend than in PP/SBS blend. Therefore, the incorporation of clay particles to small rubber particles ($<0.5 \mu\text{m}$) that cannot readily cavitate is a means to facilitate cavitation process to promote shear yielding in the PP matrix.



(b)



(c)

Figure 9 (Continued).

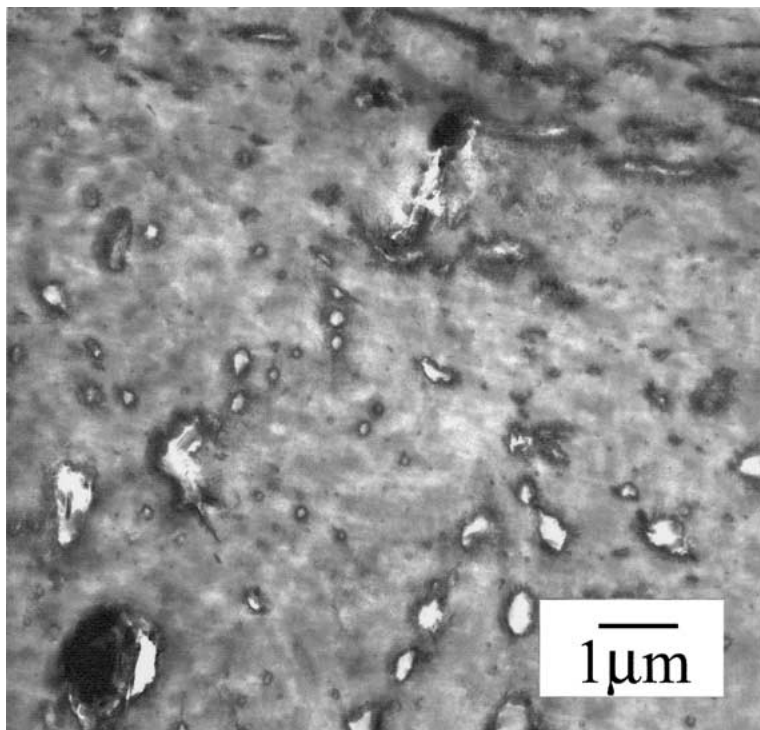


Figure 10 TEM micrograph of DN-4PB specimen of PP/SBS/clay taken at 30 μm below fracture surface.

4. Conclusion

Fracture mechanisms in PP, PP/SBS, PP/clay, and PP/SBS/clay systems are investigated. Only crack deflection and crack bifurcation are found in PP/clay system. Crazing is not observed in PP/SBS and PP/SBS/clay blends, probably due to the small particle size ($<0.5 \mu\text{m}$) of the toughener phase. Fracture toughness of PP can be best improved by clay-modified small rubber particles. Debonding between the clay inclusion and the SBS rubber phase, which is equivalent to cavitation of rubber, leads to effective relief of tri-axial stress state around the crack tip in PP/SBS/clay. This, in turn, promotes large scale shear yielding in the PP matrix. Signs of clay layer separation due to high degree of shear deformation around the crack tip region are observed.

Acknowledgments

The authors would like to thank Dr. C. Huang for assisting the sample preparation and Mr. E. I. Garcia-Metitin for the training of the TEM work. The financial supports from ATC Corporation and Defense Logistic Agency are greatly appreciated.

References

1. B. Z. JANG, D. R. UHLMANN and J. B. V. SANDE, *Polym. Eng. Sci.* **25** (1985) 643.
2. B. Z. JANG, *J. Appl. Polym. Sci.* **30** (1985) 2485.
3. H. H. KAUSCH, R. GENSLER, C. H. GREIN, C. J. G. PLUMMER and P. SCARAMUZZINO, *J. Macromol. Sci.-Phys.* **B 38**(5/6) (1999) 803.

4. Y. YOKOYAMA and T. RICCO, *Polymer* **39** (1998) 3675.
5. G.-X. WEI and H.-J. SUE, *Polym. Eng. Sci.* **40** (2000) 1979.
6. G.-M. KIM and G. H. MICHLER, *Polymer* **39** (1998) 5699.
7. R. GENSLER, Ph.D. thesis 1863, EPFL, Lausanne, Switzerland, 1998.
8. A. VAN DER WAL and R. J. GAYMANS, *Polymer* **40** (1999) 6067.
9. *Idem.*, *ibid.* **40** (1999) 6031.
10. *Idem.*, *ibid.* **40** (1999) 6057.
11. A. F. YEE and R. A. PEARSON, *J. Mater. Sci.* **21** (1986) 2462.
12. *Idem.*, *ibid.* **21** (1986) 2475.
13. A. F. YEE, D. LI and X. LI, *ibid.* **28** (1993) 6392.
14. G.-X. WEI, H.-J. SUE, J. CHU, C. HUANG and K. GONG, *Polymer* **41** (2000) 2947.
15. *Idem.*, *J. Mater. Sci.* **35** (2000) 555.
16. G.-M. KIM, G. H. MICHLER, J. ROSCH and R. MILHAUPI, *Acta Polymer* **49** (1998) 88.
17. G. RADONJIC, *J. Appl. Poly. Sci.* **72** (1999) 291.
18. H. X. NGUYEN and H. ISHIDA, *Polym. Compos.* **8** (1987) 57.
19. H. MENENDEZ and J. L. WHITE, *Polym. Eng. Sci.* **24** (1984) 1051.
20. M. C. LEE and C. H. TENSA, *J. Adhes. Sci. Tech.* **3** (1989) 291.
21. W. Y. CHIANG, W. D. YANG and B. PUKANSZKY, *Polym. Eng. Sci.* **32** (1992) 641.
22. Y.-C. OU, T.-T. GUO, X.-P. FANG and Z.-Z. YU, *J. Appl. Polym. Sci.* **74** (1999) 2397.
23. Y. LONG and R. A. SHANKS, *ibid.* **61** (1996) 1877.
24. J. KOLARIK and J. JANCAR, *Polymer* **33** (1992) 4961.
25. J. BRANDUP, in "Polymer Handbook" (Wiley, New York, 1975).
26. A. T. JONES, J. M. AIZLEWOOD and D. R. BECKETT, *Makromo. Chem.* **75** (1964) 134.
27. J. LU, G.-X. WEI, H.-J. SUE and J. CHU, *J. Appl. Polym. Sci.* **76** (2000) 311.

Received 26 June 2001

and accepted 29 January 2002